Large closed-field corona of WX Ursae Majoris evidenced from radio observations

Davis, I.; Vedantham, H.K.; Callingham, J.R.; Shimwell, T.W.; Vidotto, A.A.; Zarka, P.; ... ; Drabent, A.

Large closed-field corona of WX UMa evidenced from radio observations

I. Davis[1,2], H. K. Vedantham[1,3], J. R. Callingham[1,4], T. W. Shimwell[1,4], A. A. Vidotto[5], P. Zarka[6], T. P. Ray[7], and A. Drabent[8]

1 ASTRON, Netherlands Institute for Radio Astronomy, Oude Hoogeveensedijk 4, Dwingeloo, 7991 PD, The Netherlands
2 Department of Physics and Astronomy, University of New Mexico, Albuquerque, USA
3 Kapteyn Astronomical Institute, University of Groningen, PO Box 72, 97200 AB, Groningen, The Netherlands
4 Leiden Observatory, Leiden University, PO Box 9513, 2300 RA, Leiden, The Netherlands
5 School of Physics, Trinity College Dublin, the University of Dublin, Dublin-2, Ireland
6 LESIA, CNRS – Observatoire de Paris, PSL 92190, Meudon, France
7 Dublin Institute for Advanced Studies, Ireland
8 Thüringer Landessternwarte, Sternwarte 5, 07778 Tautenburg, Germany

ABSTRACT

The space-weather conditions that result from stellar winds significantly impact the habitability of exoplanets. The conditions can be calculated from first principles if the necessary boundary conditions– namely on the plasma density in the outer corona and the radial distance at which the plasma forces the closed magnetic field into an open geometry– are specified. Low frequency radio observations ($\nu \lesssim 200\,\mathrm{MHz}$) of plasma and cyclotron emission from stars probe these magneto-ionic conditions. Here we report the detection of low-frequency ($120 - 167\,\mathrm{MHz}$) radio emission associated with the dMe6 star WX UMa. If the emission originates in WX UMa's corona, we show that the closed field regions extends to at least ≈ 10 stellar radii, that is about a factor of a few larger than the solar value, and possibly to $\gtrsim 20$ stellar radii. Our results suggest that the magnetic-field structure of M dwarfs is in between Sun-like and planet-like configurations, where compact over-dense coronal loops with X-ray emitting plasma co-exist with a large-scale magnetosphere with lower plasma density and closed magnetic geometry.

Key words. Stars: coronae – Radio continuum: stars – Plasmas – Radiation mechanisms: non-thermal

1. Introduction

M-dwarfs often host multiple terrestrial temperate exoplanets (Dressing & Charbonneau 2015; Gillon et al. 2017). Since M-dwarfs display heightened levels of magnetic activity over gigayear timescales, their high energy photon and plasma ejection could adversely affect the habitability of exoplanets (Kopparapu et al. 2013).

Magnetohydrodynamical (MHD) simulations of exoplanet space-weather have been used to model the interplanetary plasma density and magnetic field strength around low-mass stars (Vidotto 2021; Vidotto et al. 2013; Cohen et al. 2014; Garraffo et al. 2017). These models must necessarily ascribe boundary conditions on the plasma density and velocity, as well as the magnetic field strength and topology on some closed surface. The large-scale magnetic field at the stellar surface can be well constrained by Zeeman Doppler imaging maps (Morin et al. 2010) but the radial evolution of the field, and the radius at which it transitions from a closed topology to radially distended open topology, cannot be determined without explicit knowledge of the plasma density. The plasma density in these simulations is usually assumed ad-hoc or estimated from the X-ray luminosity of the star. However, the X-ray measurements are likely biased towards over-dense gas that is held confined in short coronal loops (smaller than the stellar radius typically) since X-ray emissivity depends on the square of the electron density. Instead, it is the lower density plasma that occupies the bulk of the coronal volume that expands as the stellar wind. The density contrast between plasma in short coronal loops and the bulk of the corona could, in principle, be orders of magnitude on M-dwarfs because their intense magnetic fields can support such a pressure difference (see Pneuman 1968, for a theoretical analysis of a generic open-closed field boundary region). As a result, existing MHD simulations have been hampered by a lack of empirically determined boundary conditions for the coronal gas properties.

Polarised lower frequency radio emission, due to the plasma or cyclotron maser mechanism, is expected to originate at much higher coronal layers (many stellar radii as we demonstrate here) instead of from short coronal loops close to the stellar surface where the densest X-ray emitting gas is thought to be confined. Such radio observations can therefore provide a crucial constraint on the density of the outflowing plasma and significantly improve the reliability of exoplanet space-weather simulations.

The vast majority of stellar radio emission has only been studied at frequencies greater than 1 GHz (Güdel 2002) owing mainly to sensitivity constraints. The advent of sensitive radio telescopes at metre wavelengths has opened up the low-frequency window to stars and brown dwarfs (Lynch et al. 2017; Villadsen & Hallinan 2019; Vedantham et al. 2020c; Callingham et al. 2021a; Vedantham et al. 2020a). As part of our ongoing effort to constrain coronal parameters using low-frequency emission, here we focus on WX UMa— a system blindly detected (Callingham et al. 2021b) in the ongoing Low-Frequency Ar-

ray (LOFAR) Two-metre Sky Survey (LoTSS) (Shimwell et al. 2017, 2019) with the LOFAR telescope (van Haarlem et al. 2013). We have chosen WX UMa from our LoTSS detected stars because its magnetic field strength and topology are well known (Morin et al. 2010). Here we use the LOFAR radio data to show that, if the emission originates in the corona of WX UMa, then the low frequency of emission, despite the strong magnetic field of WX UMa, requires the star to have a closed-field configuration out to a radial distance of $\gtrsim 10$ stellar radii and possibly $\gtrsim 20$ stellar radii. This is substantially larger than radial distances to the open-closed field boundary of $3 - 5$ stellar radii that has been derived from existing MHD simulations of M-dwarfs stellar winds (Vidotto et al. 2013, 2014; Kavanagh et al. 2021), but comparable to the size of 'slingshot prominences' (Collier Cameron & Robinson 1989) proposed to exist on fast-rotating cool stars (Jardine et al. 2020).

2. Observations & Results

2.1. Low-frequency radio detection

WX UMa was discovered as a radio source in the 120-168 MHz LoTSS survey (Callingham et al. 2021b) as part of our on-going blind survey for stellar, brown dwarf and planetary radio emission (Vedantham et al. 2020c,b; Callingham et al. 2019, 2021a). LoTSS surveys the sky with a tessellation of partially overlapping pointings (Shimwell et al. 2017, 2019). WX UMa was observed in four such pointings (see Table 1 and Fig. 1). However, two of the four pointings were observed simultaneously using LOFAR's multi-beaming capability and therefore have redundant information between them. The source is detected in all three independent pointings and has a consistently high ($\gtrsim 70\%$) circular polarisation fraction when averaged over the full ≈ 8 h of each observation. Its companion star, GJ 412 A that is $\approx 30''$ away, is not detected in any pointing.

2.2. Spectro-temporal properties

The low frequency radio emission from WX UMa is broad-band and persistent. The emission persists for most of the 8 hr observation block in each exposure, as seen in Fig. 2. The spectrum, shown in Fig. 3 is particularly interesting, as it has a consistent shape across the observations: it is bright at the low-end of the observational band, and rapidly declines within a few MHz around ≈ 150 MHz to a level below our detection threshold. For instance, in the 2016-03-22 exposure (P167+42), for which we have the best Stokes-V sensitivity, the emission changes from $\approx -1500 \mu$Jy at 124 MHz to being undetectable (below 3σ) in the three 7.8-MHz wide channels between ≈ 148 to ≈ 170 MHz, which have an rms noise of $\approx 140 \mu$Jy. This corresponds to a factor of ≈ 4 decline over a fractional bandwidth $\Delta\nu/\nu \approx 0.15$, where ν is the observing frequency. The decline in other epochs appears to be even more abrupt. However, the available signal-to-noise does not allow us to trace the spectral decline in finer channels. The small number of exposures (three) also do not allow a meaningful search for patterns in the location of the spectral turnover with observation epoch.

We also averaged the images in the three 7.8-MHz channels of the P167+42 that yielded non detections at the 3σ level. The averaged image (not shown here) revealed a faint 3.5σ source at the location of WX UMa. This suggests that the emission may settle into a low plateau as opposed to a total cut-off. Hence, despite the rapid decline, the emission does not appear to 'turn-off' entirely at the high frequency end of our band.

Further details of the radio data processing and extraction of dynamic spectra are given in Appendix A.

3. Discussion

The known properties of WX UMa which will aid in our interpretation of the radio emission are summarised in Table 2. Because the emission is persistent, we only consider cases where the emitting plasma is trapped within a closed magnetic geometry. This is because plasma that unbinds from the star is expected to expand on a timescale that is much shorter than the duration of our observations. For example, solar radio emission from plasma flowing along open field lines typically lasts seconds to minutes as seen in solar Type-II and Type-III bursts (Wild & Smerd 1972).

Magnetically trapped plasma in stellar coronae can emit via different mechanisms depending on the energy of the emitting electrons and the ambient magneto-ionic parameters (Dulk 1985). The high circular polarisation fraction rules out all known incoherent emission mechanisms. Coherent emission mechanisms that can generate up to 100% circularly polarised emission are fundamental plasma emission and fundamental and second harmonic cyclotron emission. While cyclotron emission occurs at the harmonics of the electron cyclotron frequency (Treumann 2006; Melrose & Dulk 1982), plasma emission in a magnetic trap is thought to occur at the harmonics of the upper hybrid frequency (Zaitsev & Stepanov 1983; Stepanov et al. 2001) which is the quadrature sum of the plasma and electron cyclotron frequencies. Both of these mechanisms can account for the long duration of the observed emission. Plasma emission will persist for as long as the turbulent Langmuir wave spectrum that powers the emission is maintained. CMI from ultracool dwarfs is commonly seen to be pulsed at the rotation period due to beaming, but for conducive geometries, it can be visible at all rotation phases. CMI's beaming geometry is discussed in more detail in §3.6 and Appendix C.

3.1. Emission site

The magnetic field of WX UMa is largely dipolar with a polar surface magnetic field strength of ≈ 4.5 kG (Morin et al. 2010). This yields a maximum cyclotron frequency at the surface of ≈ 12.6 GHz. Because a dipolar field evolves with radial distance R as R^{-3}, fundamental cyclotron emission in the observed frequency band can only originate at a radial distance of $\approx 4.7R_*$, where R_* is the stellar radius.

If the emission is due to the plasma mechanism, the emission site cannot be accurately pinpointed because the plasma density profile in WX UMa is not known apriori. However, a lower bound on the radial distance of the emission site can be placed based on the requirement for radiation escape. Escaping radiation in the presence of cyclotron damping is obtained when the ambient cyclotron frequency is sufficiently low: $\nu_c < 0.26\nu_p$ (see Appendix B). Observable plasma emission at 120 MHz therefore requires the ambient magnetic field to be below ≈ 11 G. For a dipolar field that evolves with radial distance as R^{-3}, this value can only be reached on WX UMa for $R > 7.4R_*$. We note that although there is a narrow window of low cyclotron opacity at small angles to the magnetic field for $\nu_c > 0.26\nu_p$ (see Fig. A1 of Vedantham 2020), the bulk of the radiation will still be absorbed since spontaneous plasma emission is quasi-isotropic.

LoTSS field	Obs. date	Dist.	Obs. id	Stokes-I (mJy)	Stokes-V (mJy)	Pol. fraction
P5Hetdex	2014-09-07	1°.81	233996	1.8(2)	−1.4(2)	0.8(1)
P167+42	2016-03-22	1°.54	441476	0.6(1)	−0.58(6)	1.0(1)
P163+45*	2015-11-11	2°.32	403966	1.1(1)	−0.8(1)	0.7(1)
P163+42*	2015-11-11	2°.31	403966	0.9(1)	−0.6(1)	0.7(1)

Table 1. Details of LOFAR observations of WX UMa. Quantities in brackets denote 1σ root mean square (rms) uncertainty on the least significant digit. WX UMa is seen through different gains in the primary beam which leads to differing noise levels. The polarised fraction error is computed by Taylor expanding the ratio to first order. The two exposures with an * superscript were taken concurrently using LOFAR's multi-beam capability.

Parameter	Value	Reference/Comments
Spectral class	dM6e	Alonso-Floriano et al. (2015)
Mass ($M_\odot$)	0.095	Newton et al. (2017)
Radius ($R_\odot$)	0.12	Morin et al. (2010)
Distance (pc)	4.9	Gaia Collaboration et al. (2018)
ROSAT X-ray luminosity (ergs s^{-1})	3.62×10^{27}	Callingham et al. (2021b)
Hα equivalent width (Å)	6.85 ± 0.09	Newton et al. (2017)
Surface polar magnetic field* (kG)	4.53	Morin et al. (2010)
Stellar rotation period (days)	0.78	Morin et al. (2010)
Average coronal temperature	5.8×10^6 K	Based on Johnstone & Güdel (2015)
Density scale height	$0.63R_*$	Neglecting centrifugal force

Table 2. Known properties of WX UMa from literature. *Morin et al. (2010) also found that the magnetic field is well described by a dipole: $B = (B_0/2)R^{-3}(2\cos\theta\hat{r} + \sin\theta\hat{\theta})$, where B_0 is the polar surface field strength, R is the radial distance in units of the stellar radius, θ is the polar angle, and $\hat{r}$ and $\hat{\theta}$ are the unit vectors along the radial and polar-angular directions.

3.2. Polarisation parity

The Zeeman doppler imaging (ZDI) maps of WX UMa show the star to have an intermediate inclination with a small magnetic obliquity and the south magnetic pole pointed towards us (i.e. field lines pointed towards the star; Morin et al. 2010). The observed radio emission is right-hand circularly polarised (see Appendix A.1 for details of sign convention). It is therefore in the o-mode if it originates in the polar regions (where the field points away from us) and x mode if it originates in the equatorial regions (where the field points towards us). Fundamental plasma emission is polarised in the o-mode, whereas cyclotron maser emission can be polarised in the x-mode or o-mode depending on the ambient plasma density (Dulk 1985; Vedantham 2020). Because WX UMa has a mostly axisymmetric dipolar field (Morin et al. 2010), we use cyclotron maser emission from Jupiter as a benchmark for our discussion for the possibility of cyclotron maser emission from WX UMa (Zarka 1998). Following this, the unstable electron distribution in a closed field region necessary to drive the cyclotron maser is expected to be situated close to the magnetic poles, and therefore, we only consider o-mode cyclotron emission. The o-mode cyclotron maser for a loss-cone distribution is expected to dominate for $0.1 \lesssim v_c/v_p \ll 1$, with the x mode dominating at lower plasma densities ($v_c/v_p \lesssim 0.1$) (Hewitt et al. 1982; Melrose & Dulk 1982). In summary, the observed polarity requires the emission to originate in the polar regions and be driven by either fundamental plasma emission, or o-mode cyclotron maser emission in which case $v_c/v_p \gtrsim 0.1$.

3.3. Extent of the closed field region

To recap, the two possibilities for the emission mechanism are: (a) plasma emission at a radial distance of $> 7.4R_*$ with ambient density of $\approx 2 \times 10^8$ cm^{-3}, and (b) cyclotron maser at a radial distance of $4.7R_*$ with ambient density of $\gtrsim 2 \times 10^6$ cm^{-3}. Detailed MHD simulations are necessary to use these constraints to determine the size of the closed field region accurately, but we can

place preliminary constraints with simplifying assumptions. Let us assume that the density has a hydrostatic profile with the inclusion of the centrifugal force (see eqn. 3 of Havnes & Goertz 1984). We then use the dipolar structure of the magnetic field and compute the equatorial distance at which the gas pressure (nk_BT where T is the temperature, n is the number density and k_B is Boltzmann's constant), is equal to the magnetic pressure. Beyond this radial distance, we assume that the gas forces open the field lines. So we identify this radial distance as the radius of the closed field region. Using this procedure and values relevant for WX UMa from table 2 we find that the closed-open boundary occurs at radii of $\approx 10R_*$ and $22R_*$ for the case of fundamental plasma emission and cyclotron emission respectively. Finally, the co-rotation radius, $R_C = (GM/\Omega^2)^{1/3}$ (G is the gravitational constant, Ω is the angular speed, M is the stellar mass) is about $13.6R_*$ for WX UMa. It is noteworthy that the corotation radius is comparable to the approximate open-closed boundary for the case of plasma emission.

3.4. Source of emitting electrons

With these considerations, it is still presently unclear what the source of the emitting electrons is in WX UMa, but we can draw analogies with two known systems. We first consider the solar paradigm for the case of plasma emission. In this case, the ultimate energy source is thought to be magnetic reconnection in coronal loops close to the surface (Priest & Forbes 2002). However, the brightness temperature arguments in Sec. 3.5 show that the solar paradigm can only apply to WX UMa if its entire coronal volume out to a radial distance of $\gtrsim 7.4R_*$ is filled with flaring loops which is unprecedented. We may alternatively adopt the Jovian paradigm, where cyclotron maser emission is emitted by suprathermal electrons (Dulk 1985) that are accelerated by breakdown of co-rotation between the magnetic field and the magnetospheric plasma far from the planet's surface, or by unipolar induction by its moons (Goldreich & Lynden-Bell 1969). A similar acceleration mechanism sited in the equatorial

plasma sheet at few tens of stellar radii may be responsible for WX UMa's radio emission. Such an acceleration mechanism has also been suggested for magnetic chemically peculiar stars (Linsky et al. 1992). It it also noteworthy that both WX UMa and magnetic chemically peculiar stars have strong large scale magnetic fields, hot X-ray coronae and emit coherent circularly polarised emission (e.g. CU Vir, Trigilio et al. 2000).

3.5. Brightness temperature

The brightness temperature of the radio emitter assuming isotropic emission is $T_b \approx 10^{12.5} x^{-2}$ K where x is the radius of the emitter in units of the stellar radius. Theory allows the brightness temperature of cyclotron maser emission to be many orders of magnitude higher than this value (Treumann 2006; Melrose & Dulk 1982), and hence, the observed value can be readily accommodated. Fundamental plasma emission on the other hand cannot attain brightness temperatures $\gg 10^{12}$ K, especially at such low frequencies (Vedantham 2020). As shown in §3.1, the projected source radius for plasma emission is $x \approx 7.4$, giving an observed brightness temperature of $\sim 10^{11}$ K. Although we note there is no precedence for plasma emission to be simultaneously occurring at this brightness throughout the corona (at $x = 7.4$ in this case), such a brightness temperature can be reached by plasma emission based on canonical theory if the plasma is highly turbulent (see Appendix A.1). Therefore, brightness temperature arguments do not provide a clear discriminant between the two plausible emission mechanisms.

3.6. Origin of the spectral evolution

Coherent stellar and planetary radio emission are known to display narrowband spectral features but their frequency centroid generally varies stochastically with time (see Litvinenko et al. 2009; Villadsen & Hallinan 2019, for examples).[1] As such, the rapid spectral evolution from WX UMa is not unusual, but the persistent location of the spectral turn-over is noteworthy. The persistence suggests that it encodes meaningful information on the nature and geometry of emission.

The expressions for the emissivity and absorption coefficients of various emission processes themselves vary smoothly, to polynomial order, with frequency (Zheleznyakov 1996). We must therefore seek an explanation for the rapid spectral evolution in terms of beaming, resonance conditions or abrupt boundaries over which the plasma properties can change substantially. With this in mind, we consider three plausible explanations.

– *Beaming:* If the emission is driven by the cyclotron maser mechanism, then a natural explanation for the cut-off would be due to beaming of the emission. Cyclotron maser emission is beamed into a hollow cone with a large opening angle, $\theta \lesssim \pi/2$, small thickness, $\Delta\theta \ll \theta$ and whose axis is parallel to the ambient magnetic field. Radiation cones axes on a given field line make smaller angles with the magnetic axis at larger frequencies as illustrated in Fig. 4. Hence it is possible to construct geometries where the emission goes out of sight at higher frequencies. For example, consider emission originating on field lines that intersect the equatorial plane at some radius L. If the magnetic field line makes a polar angle $\alpha(\nu)$ at the point where emission at frequency ν

originates, then the emission will be visible to all observers within a magnetic co-latitude 'visibility band' that lies between $\theta - \alpha(\nu) - \Delta\theta$ and $\theta + \alpha(\nu) + \Delta\theta$. If $\alpha(\nu)$ evolves sufficiently rapidly with ν, then a spectral cut off can be explained by beaming. Could a spectral evolution be observed due to the visibility-band edge moving over the line of sight to the Earth within the observed frequency range? The function $\alpha(\nu)$ can be computed for a given L, surface magnetic field strength and dipolar geometry. For the case of LOFAR-band emission from WX UMa, the slope $\partial\alpha(\nu)/\partial\nu$ varies between $0°.05 \, \mathrm{MHz}^{-1}$ and $0°.12 \, \mathrm{MHz}^{-1}$ as L is varied between $20R_*$ and $6R_*$ (further details in Appendix). This corresponds to a shift in the visibility band by $1°$ and $2°.4$ within a 20 MHz band within the observed frequency range. The angular shift is significantly smaller than the characteristic width of the emission cone's surface, $\Delta\theta$ (Zarka 1998; Melrose & Dulk 1982) as well as other geometric parameters such as magnetic obliquity. Hence, an apparent cutoff due to beaming is possible but with a somewhat contrived geometric setup. Nevertheless, the beaming hypothesis can be tested by a search for a characteristic rotation and spectral modulation of the radio light curves at the rotation rate of WX UMa, which is an expected result of any magnetic obliquity in the system.

– *Resonant cyclotron absorption:* If the emission is due to fundamental plasma emission, then the cut-off could be due to resonant cyclotron absorption of higher frequency emission that originates deeper in the corona. This is possible because the cyclotron frequency evolves with radial distance as R^{-3} whereas the plasma frequency can evolve much more gradually with radial distance, particularly if the density scale height is large. In such a situation, it is possible for the radiation escape condition to be satisfied at larger radii where lower frequency emission originates, but not at lower radii, where higher frequency emission originates, leading to a cut-off. Fig. 5 shows plausible hydrostatic density profiles along different field lines, each with a different base density that leads to catastrophic cyclotron absorption within the LOFAR band. The density profiles all require that the base coronal density is restricted to a narrow range of values (about a 10% range) around $10^{9.1}$ cm^{-3} which is comparable to the solar value. If this is the correct mechanism, then similar emission (long duration, highly polarised) must not be visible from WX UMa at frequencies above the LOFAR band and long term monitoring should not show clear signs of rotation modulation in the LOFAR-band intensity. We note that WX UMa is detected between 2 and 4 GHz in the ongoing VLASS survey (Lacy et al. 2020) at a flux density of 1.3(1) mJy.[2] However, the VLASS survey observes with 3 minute exposures which is not long enough to associate the VLASS-detected emission with the long duration LOFAR-detected emission as opposed to a shorter duration burst.

– *Surface cut-off*: The rapid spectral evolution can be explained if the bulk of the emission does not originate in WX UMa's corona but instead in the magnetosphere of a closeby (unresolved) sub-stellar companion and the cut-off frequency corresponds to a cyclotron frequency consistent with a surface magnetic field strength of ~ 40 G, much in the same way Jovian cyclotron emission cuts-off at around 40 MHz. This would be an unprecedented conclusion if true, as it would amount to a radio discovery of a sub-stellar companion (exoplanet or brown dwarf) around WX UMa. A prediction of

---

[1] A possible exception is AD Leo whose bursts observed by Villadsen & Hallinan (2019) show an apparent cut-off near-consistently around 1.5 GHz.

[2] Based on the VLASS 'quick-look' images. See https://science.nrao.edu/science/surveys/vlass

this interpretation is periodic rotational modulation of the radio emission at a rate that does not match the known rotation rate of WX UMa. However, this property cannot be inferred from the current data since the emission has been detected in all three independent pointings.

In summary, we have identified three possible mechanisms to explain the rapid spectral evolution all of which can be tested with monitoring the LOFAR-band emission over several rotation cycles and with gigahertz frequency observations.

4. Summary and outlook

We have detected persistent highly circularly polarised ($\gtrsim 70\%$) radio emission around $144\,\mathrm{MHz}$ from WX UMa. If the emission originates from WX UMa's corona, there are two plausible emission mechanisms that can account for the radio emission: (a) plasma emission at the fundamental at a radial distance of $\gtrsim 7.4R_*$ where the ambient plasma density is $\approx 10^{8.5}\,\mathrm{cm}^{-3}$, and (b) o-mode cyclotron maser emission in which case the emission originates at a radial distance of $\approx 4.7R_*$ where the ambient coronal density is $10^{6.5}\,\mathrm{cm}^{-3}$.

We expect our plasma density constraints to provide guidance to MHD simulations of the stellar wind of WX UMa. A simple balance between gas and magnetic pressure yield the radial extant of the closed field regions to be $\approx 10R_*$ (plasma emission) and $\approx 22R_*$ (cyclotron emission) respectively. Such radii are substantially larger than those that have been inferred from several MHD wind simulations of M-dwarfs (see for e.g. Vidotto et al. 2014), but are comparable to recent simulation of M-dwarf winds with low mass-loss rates (Kavanagh et al. 2021). Interestingly, the closed−open field boundary in the equatorial plane for the plasma emission model is close to the co-rotation radius for WX UMa which is the anticipated extent of slingshot prominences (Jardine et al. 2020).

WX UMa's radio spectrum shows a rapid decline within the observing band which could be a result of beaming of cyclotron emission or due to cyclotron absorption of plasma emission. Alternatively, the radio emission we observe might have originated not on WX UMa but on a sub-stellar companion. All three possibilities can be tested with longer term multi-frequency monitoring of WX UMa's radio emission.

References

Alonso-Floriano, F. J., Morales, J. C., Caballero, J. A., et al. 2015, A&A, 577, A128
Callingham, J. R., Pope, B. J. S., Feinstein, A. D., et al. 2021a, arXiv e-prints, arXiv:2102.04751
Callingham, J. R., Vedantham, H. K., Pope, B. J. S., Shimwell, T. W., & LoTSS Team. 2019, Research Notes of the American Astronomical Society, 3, 37
Callingham, J. R., Vedantham, H. K., Shimwell, T. W., & Pope, B. J. S. 2021b, Nature Astronomy (under review), xxx, xxx
Cohen, O., Drake, J. J., Glocer, A., et al. 2014, ApJ, 790, 57
Collier Cameron, A. & Robinson, R. D. 1989, MNRAS, 238, 657
Dressing, C. D. & Charbonneau, D. 2015, ApJ, 807, 45
Dulk, G. A. 1985, ARA&A, 23, 169
Gaia Collaboration, Brown, A. G. A., Vallenari, A., et al. 2018, A&A, 616, A1
Garraffo, C., Drake, J. J., Cohen, O., Alvarado-Gómez, J. D., & Moschou, S. P. 2017, ApJ, 843, L33
Gillon, M., Triaud, A. H. M. J., Demory, B.-O., et al. 2017, Nature, 542, 456
Goldreich, P. & Lynden-Bell, D. 1969, ApJ, 156, 59
Güdel, M. 2002, ARA&A, 40, 217
Hancock, P. J., Murphy, T., Gaensler, B. M., Hopkins, A., & Curran, J. R. 2012, MNRAS, 422, 1812
Havnes, O. & Goertz, C. K. 1984, A&A, 138, 421
Hewitt, R. G., Melrose, D. B., & Ronnmark, K. G. 1982, Australian Journal of Physics, 35, 447
Jardine, M., Collier Cameron, A., Donati, J. F., & Hussain, G. A. J. 2020, MNRAS, 491, 4076
Johnstone, C. P. & Güdel, M. 2015, A&A, 578, A129
Kavanagh, R. D., Vidotto, A. A., Klein, B., et al. 2021, MNRAS[arXiv:2103.16318]
Kopparapu, R. K., Ramirez, R., Kasting, J. F., et al. 2013, ApJ, 765, 131
Lacy, M., Baum, S. A., Chandler, C. J., et al. 2020, PASP, 132, 035001
Linsky, J. L., Drake, S. A., & Bastian, T. S. 1992, ApJ, 393, 341
Litvinenko, G. V., Lecacheux, A., Rucker, H. O., et al. 2009, A&A, 493, 651
Lynch, C. R., Lenc, E., Kaplan, D. L., Murphy, T., & Anderson, G. E. 2017, ApJ, 836, L30
Melrose, D. B. & Dulk, G. A. 1982, ApJ, 259, 844
Morin, J., Donati, J. F., Petit, P., et al. 2010, MNRAS, 407, 2269
Newton, E. R., Irwin, J., Charbonneau, D., et al. 2017, ApJ, 834, 85
Pneuman, G. W. 1968, Sol. Phys., 3, 578
Priest, E. R. & Forbes, T. G. 2002, A&A Rev., 10, 313
Shimwell, T. W., Röttgering, H. J. A., Best, P. N., et al. 2017, A&A, 598, A104
Shimwell, T. W., Tasse, C., Hardcastle, M. J., et al. 2019, A&A, 622, A1
Stepanov, A. V., Kliem, B., Zaitsev, V. V., et al. 2001, A&A, 374, 1072
Tasse, C., Shimwell, T., Hardcastle, M. J., et al. 2020, arXiv e-prints, arXiv:2011.08328
Treumann, R. A. 2006, A&A Rev., 13, 229
Trigilio, C., Leto, P., Leone, F., Umana, G., & Buemi, C. 2000, A&A, 362, 281
van Haarlem, M. P., Wise, M. W., Gunst, A. W., et al. 2013, A&A, 556, A2
van Straten, W., Manchester, R. N., Johnston, S., & Reynolds, J. E. 2010, PASA, 27, 104
van Weeren, R. J., Shimwell, T. W., Botteon, A., et al. 2020, arXiv e-prints, arXiv:2011.02387
Vedantham, H. K. 2020, arXiv e-prints, arXiv:2008.05707
Vedantham, H. K., Callingham, J. R., Shimwell, T. W., et al. 2020a, ApJ, 903, L33
Vedantham, H. K., Callingham, J. R., Shimwell, T. W., et al. 2020b, arXiv e-prints, arXiv:2010.01915
Vedantham, H. K., Callingham, J. R., Shimwell, T. W., et al. 2020c, Nature Astronomy, 4, 577
Vidotto, A. A. 2021, In press, Living Reviews in Solar Physics
Vidotto, A. A., Jardine, M., Morin, J., et al. 2013, A&A, 557, A67
Vidotto, A. A., Jardine, M., Morin, J., et al. 2014, MNRAS, 438, 1162
Villadsen, J. & Hallinan, G. 2019, ApJ, 871, 214
Wild, J. P. & Smerd, S. F. 1972, ARA&A, 10, 159
Zaitsev, V. V. & Stepanov, A. V. 1983, Sol. Phys., 88, 297
Zarka, P. 1998, J. Geophys. Res., 103, 20159
Zheleznyakov, V. V. 1996, Radiation in Astrophysical Plasmas, Vol. 204 (Kluwer academic publishers)
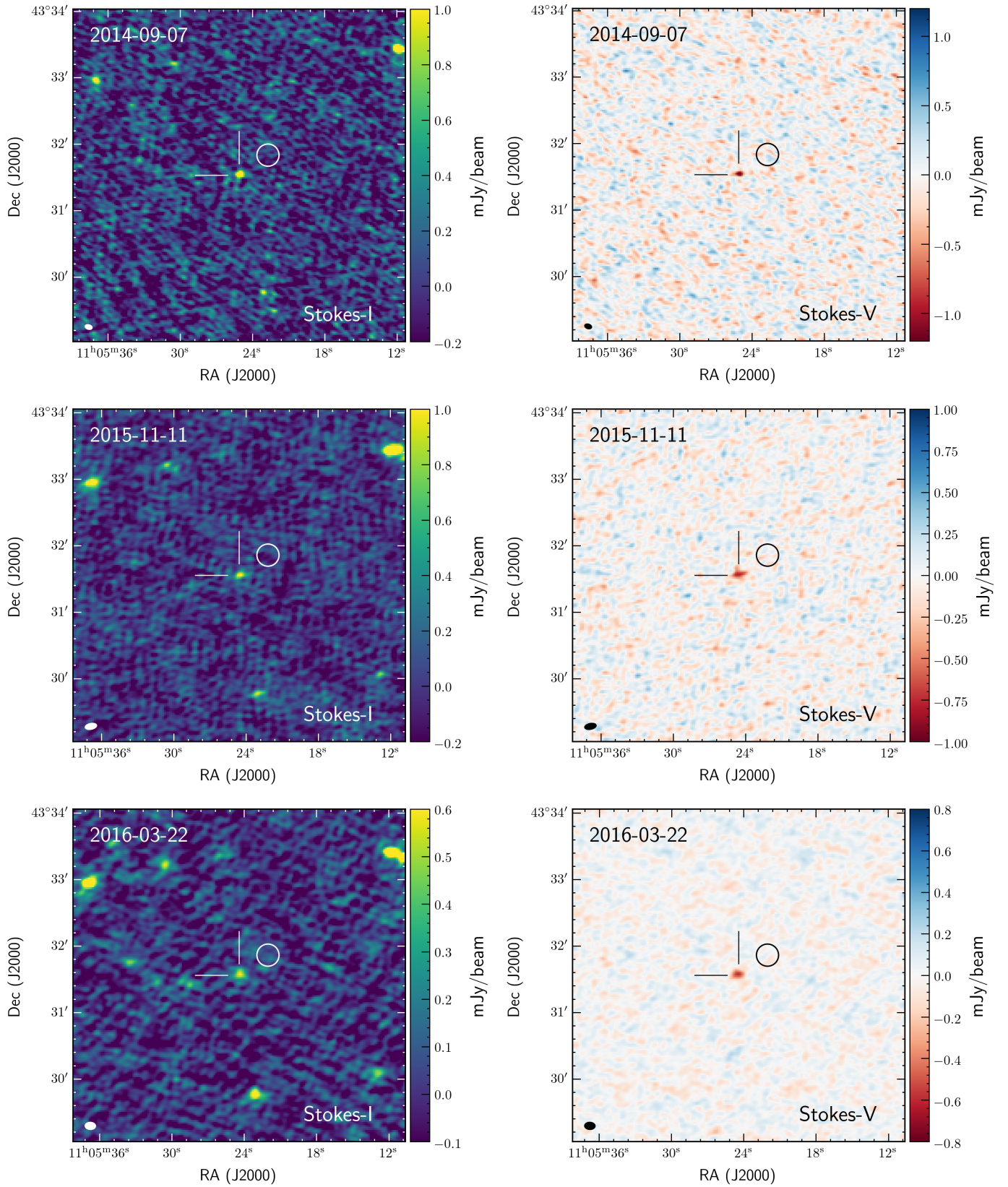
Fig. 1. Stokes-I (left) and Stokes-V (right) images of the area surrounding WX UMa. The images are formed from the entire 8 hour observation duration and entire 44 MHz bandwidth (120 − 167 MHz). The cross-hairs and circles show the proper-motion corrected position of WX UMa (GJ 412 B) and GJ 412 A, respectively, using the astrometric data from *Gaia* DR2 (Gaia Collaboration et al. 2018). The flux densities of WX UMa and uncertainties are collated in Table 1.
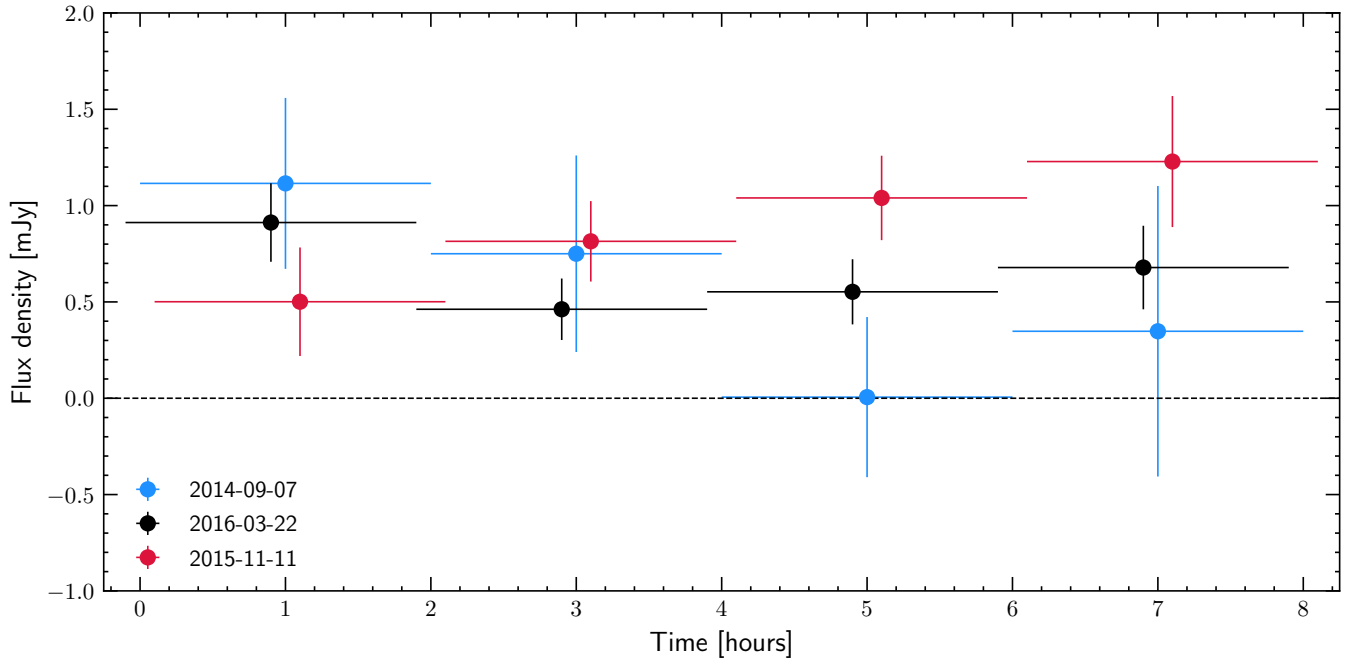
Fig. 2. Time resolved Stokes-I flux density of WX UMa averaged over the full 120-167 MHz band on the three independent exposures (see Table 1). The emission persists of most of the 8 hr survey pointing duration.
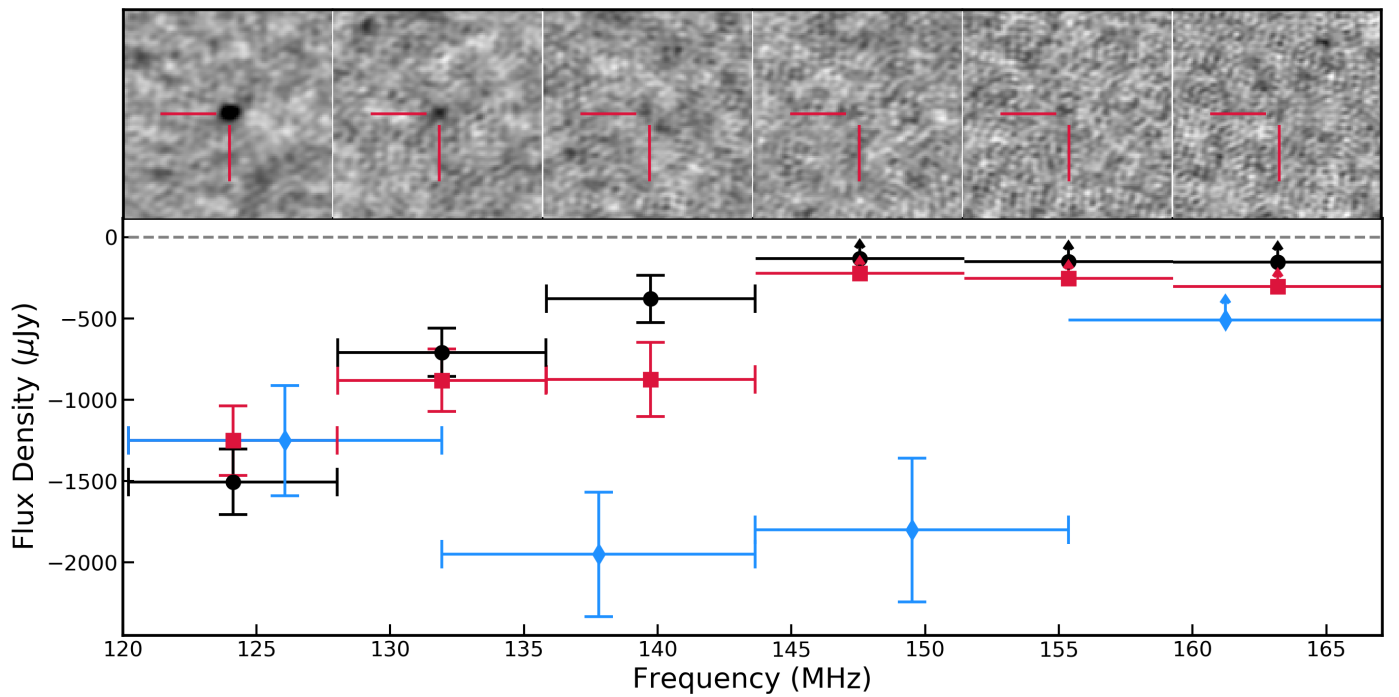

Fig. 3. Stokes-V spectrum of WX UMa in the three independent exposures from the LoTSS survey observations. The three sets of points show the spectrum for the three independent exposures. Upper limits correspond to 1σ. The grayscale images are made from the P167+42 exposure (see Table 1) over 8 hr of synthesis and ≈ 7.8 MHz of bandwidth. The red cross-hair mark the position of WX UMa. The source consistently shows a drop in flux density magnitude above ≈ 150 MHz in all epochs suggesting that this is an enduring property of the emitter. We made a 3.5-σ detection of WX UMa when averaging over the last three bands in the P167+42 observation, suggesting the spectral evolution at these higher frequencies is a low plateau rather than a cutoff.
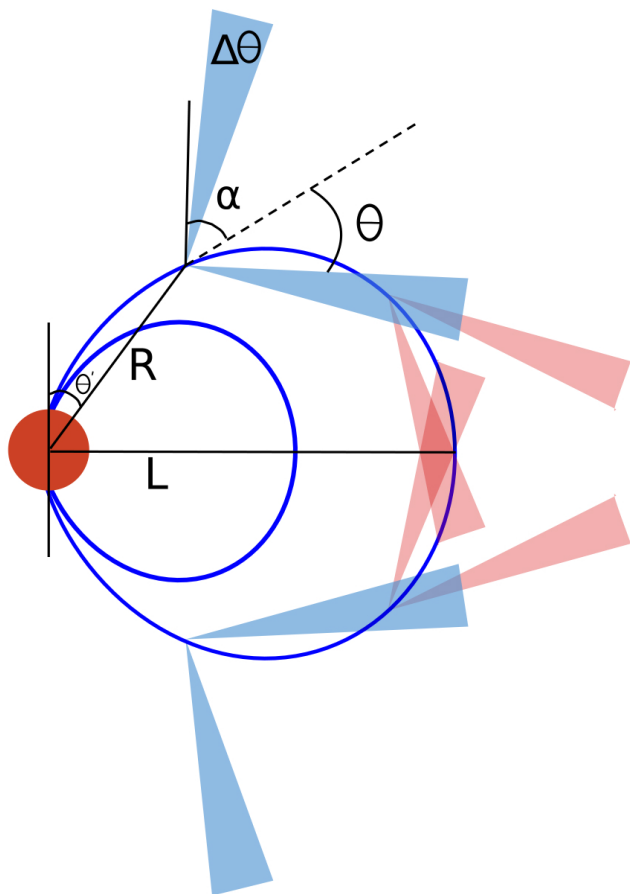
Fig. 4. A not-to-scale sketch showing the geometry of cyclotron maser emission on a single dipolar field line that lies in the plane of the page. The higher frequency emission cone (blue) is oriented at a smaller polar angle, α, when compared to the emission cone at a lower frequency (red). Here, L is the distance to the field line for a polar angle of $0°$, R is the distance from the star's centre to the emission cone along the field line, θ is the angle between the direction of emission and the interior wall of the cone, and $\Delta\theta$ is the angular width of the emission cone's wall. The effects of α and θ on emission frequency has been exaggerated here and is not to scale for the LOFAR frequency range.
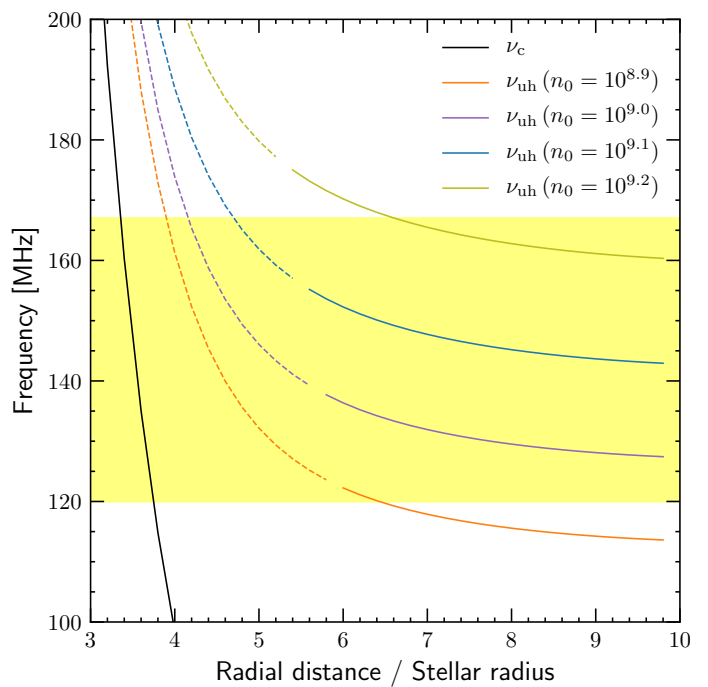

Fig. 5. Plot of the radial profile of the cyclotron frequency (solid black line) and the upper hybrid plasma frequency (coloured lines) for different base plasma density values given in units of cm^{-3}. The plasma has been assumed to follow a hydrostatic density structure along any given field-line while taking into account centrifugal force (Havnes & Goertz 1984, their equation 3). The broken lines denote regions where cyclotron absorption will preclude radiation escape. The yellow-band shows the observed frequency range.

Appendix A: Radio data processing

The data were processed with the usual LoTSS pipeline[3] (Shimwell et al. 2017, 2019) which is described in Tasse et al. (2020). We then performed an additional round of self-calibration in the direction of WX UMa with a procedure described in van Weeren et al. (2020) and also employed in (Vedantham et al. 2020c). After calibration, the measurement set was further processed to make source extraction easier for producing light curves and spectra. WX UMa was removed from the mask image which was then used to produce a model file using `WSClean`. WX UMa was also removed from these model images so that it would not be removed during the subtraction of other sources. The subtracted model image was then used with `WSClean` again to predict visibilities which were recorded in a new modelled data column in the measurement set. The modelled data was subtracted from the real data column and recorded in a new column - this served to remove all other bright sources from the region besides WX UMa. Finally, DPPP was used to phaseshift the measurement sets to be centred on WX UMa, using the subtracted data as the new real data.

After extra sources were removed from the field and the set was phaseshifted, frequency and time slices for Stokes-I and V were produced via `WSClean`. Because the signal to noise ratio of the observation was not large enough to produce a full dynamic spectrum, the frequency slices were averaged over all time and the time slices were averaged over the first 40 channels (120 to to 135.83 MHz, ≈ 16 MHz bandwidth) where WX UMa is the brightest. The Background and Noise Estimation (`BANE`) tool in `Aegean` (Hancock et al. 2012) was used with each image to produce rms and background images. `Aegean` was run with a 4σ seedclip to avoid identifying extraneous sources. The flux density for WX UMa for a particular image was assigned from the peak flux found by `Aegean` if a source was found in the expected location of WX UMa, and the rms noise was retrieved from the rms image produced by `BANE`. For images where no 4σ source was found at the star's coordinates, a priorized fitting was applied using the catalogue from the image with the most significant detection in order to extract $\approx 3\sigma$ detections at the expected position of WX UMa. The images were also inspected by eye to make sure the results of `Aegean` were consistent with the images. The temporal evolution of WX UMa's radio flux is shown in Fig. 2 and its spectral evolution is shown in Fig. 3.

We note that the some the images in the light curve estimation have non-Gaussian noise due to residual sidelobe noise (from poorer *uv* coverage) and low-level calibration errors.

Appendix A.1: Stokes-V sign convention

There are two commonly used Stokes-V sign conventions in literature. The pulsar literature typically follows the convention $V = LCP - RCP$ whereas the IAU convention is $V = RCP - LCP$ (van Straten et al. 2010). To check the convention applicable to the LoTSS images, we compared the sign of Stokes-V of several pulsar detections to that in the literature and found that the LoTSS survey data products follow the same convention as the one in pulsar literature (Callingham et al. 2021b). Hence, WX UMa is radiating RCP radiation, which means that the electric field vector rotates counter-clockwise as a function of time to an observer looking at incoming radiation.

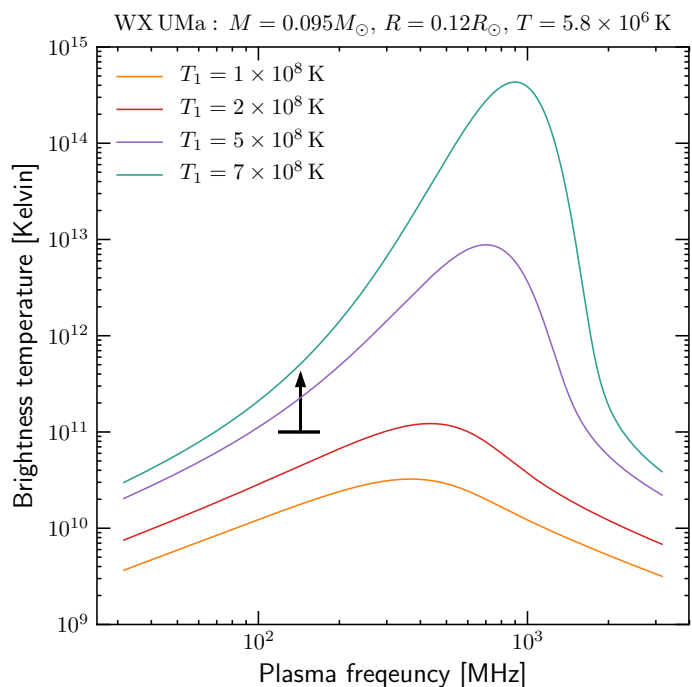[3] The LoTSS pipeline can be found at https://github.com/mhardcastle/ddf-pipeline

Fig. B.1. Brightness temperature of plasma emission computed for parameters relevant for WX UMa (annotated in the figure). The black bar is the measured value based on the radiation escape conditions and the assumption that the entire projected coronal surface is radiating.

Appendix B: Emission mechanism

Appendix B.1: Brightness temperature of plasma emission

In Fig. B.1, we computed the brightness temperature of plasma emission using the expressions of Stepanov et al. (2001, speficially, their eqn. 15). In doing so, we assumed a peak turbulence level of $w = 10^{-5}$ and to compute the plasma temperature, we used the empirical relationship of Johnstone & Güdel (2015) and the observed X-ray luminosity (Table 2).

Appendix B.2: Escape of plasma emission

Fundamental plasma emission is excited at the upper-hybrid frequency: $\nu_{uh} \approx \sqrt{\nu_p^2 + \nu_c^2}$ where ν_p and ν_c are the plasma and cyclotron frequencies respectively. Note that the upper-hybrid frequency is always larger than the cyclotron frequency. The cyclotron absorption optical depth for *o*-mode radiation propagating at an angle θ to the magnetic field may be approximated by

$$\tau = \left(\frac{\pi}{2}\right)^{5/2} \frac{2}{c} \frac{\nu_p^2}{\nu} \frac{s^{2s}}{s!} \left(\frac{k_B T \sin^2\theta}{2m_e c^2}\right)^{s-1} (1 + |\cos\theta|)^2 L_B \qquad (B.1)$$

where integer $s = \nu/\nu_c > 1$ is the cyclotron harmonic number, T is the coronal temperature, m_e is the electron mass, c is the speed of light, k_B is Boltzmann's constant and L_B is the magnetic scale length which we take to be R_*. For the parameters of interest: $T \sim 10^{6.7}$ K, $L_B \sim 10^{10}$ cm, the optical depth is safely below unity only for $s \geq 4$. Hence, the radiation escape condition is $\sqrt{\nu_p^2 + \nu_c^2} > 4\nu_c$, which gives $\nu_c < 0.26\nu_p$.
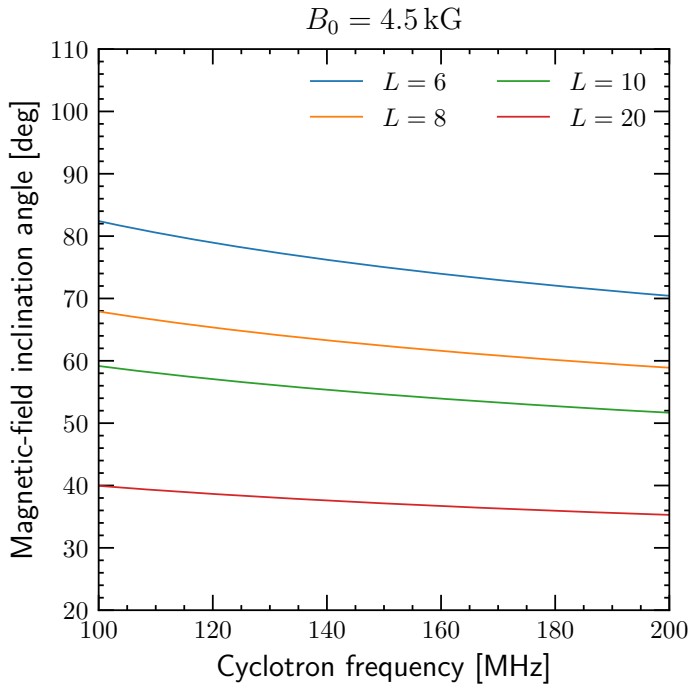
$$B_0 = 4.5\,\text{kG}$$

Fig. C.1. Polar angle of the magnetic field at the site of emission (y-axis) versus frequency of emission (x-axis) for different field lines specified by the radial distance at which they intersect the equatorial plane.

Appendix C: Spectral evolution of the emission-cone

Consider a single dipolar field line which intersects the equatorial plane at radial distance L. The radial distance and polar angle, θ' along the field line are related via $L = R\sin^2\theta'$. The polar inclination angle of the field lines, α is given by $\cos\alpha = (3\cos^2\theta' - 1)(1 + 3\cos^2\theta')^{-1/2}$. The magnetic field strength (and cyclotron frequency) vary continuously along the field line according to $\nu(R) = \nu_0 R_*^3/(2R^3)(4 - 3R/L)^{1/2}$, where ν_0 is the peak cyclotron frequency at $\theta' = 0$, $R = R_*$. With the above relationships, we predicted the inclination of the emission cone axis for various L-shell at a range of cyclotron frequencies (see Fig. C.1). The numerically computed slope of the α versus ν lines at 140 MHz vary between $\partial\alpha/\partial\nu \approx 0.2°/\text{MHz}$ and $\partial\alpha/\partial\nu \approx 0.8°/\text{MHz}$ as L is varied between 6 and 20. The magnitude of the slope decreases for larger L and must asymptote to zero as L tends to infinity.